Photoinduced Bimolecular Reactions in Homogeneous $[CH_3ONO]_n$ Clusters

K. Bergmann and J. Robert Huber*

Physikalisch-Chemisches Institut der Universität Zürich, Winterthurerstrasse 190, CH-8057 Zürich, Switzerland

Received: August 19, 1996; In Final Form: October 24, 1996[⊗]

The photodissociation of homogeneous methyl nitrite clusters, $[CH_3ONO]_n$ with $n \approx 400-1000$, was investigated in a supersonic jet using excitation mainly at 365 nm, which corresponds to $S_0 \rightarrow S_1$ ($n\pi^*$) excitation in the monomer. Besides the two types of NO($\tilde{X}^2\Pi$) photofragment distributions, a rotationally relaxed one ($T_{rot} \sim 250$ K) and a nonthermally "hot" one ($\langle J'' \rangle = 35.5$) which result from the primary dissociation step $CH_3ONO \rightarrow CH_3O + NO$ of cluster-bound CH_3ONO, we observed the products HNO($\tilde{X}^1A'$) and $H_2CO(\tilde{X}^1A_1)$ by state-selected LIF spectroscopy. Their product−yield excitation spectra and their formation dependence on the backing pressure revealed that HNO and H_2CO originate exclusively from cluster photodissociation and not from primary photodissociation of the monomer. The mechanism of their formation was found to be the disproportionation reaction of the primary photofragments, $CH_3O + NO \rightarrow HNO + H_2CO$, mediated by caging of the cluster environment. The fragments collide with, and recoil at, the solvent shell followed by subsequent recombination, disproportionation, or escape from the evaporating solvent cage. The present results are consistent with previous findings on the photolysis of isolated CH_3ONO molecules in solid noble gas matrices where exclusively the products HNO and H_2CO were found.

1. Introduction

The study of photoinduced chemical reactions in clusters has recently attracted much attention.[1−7] The aim of these investigations, which are carried out in supersonic jet expansion, is to gain deeper insight to the microscopic pathway of a chemical reaction in a "solvent" environment. The chemically reactive or inert environment acts for the initially prepared photofragments as a cage, whose influence on the subsequent reaction(s) can be studied with respect to cluster size, rigidity, or temperature. The results of such cluster studies have greatly contributed to a better understanding of the differences of the chemical processes occurring in the bulk gas-phase, the condensed-phase, and solid matrices.

The photolysis of a diatomic molecule weakly bound to chemically inert rare-gas atoms has become a prototype system to study the effect of the solvent cage on the solute fragmentation dynamics. It has been observed experimentally and theoretically that the cluster solvent cage can temporarily trap the fragments, delay their separation, or prevent it by recombination. The dissociation and cage recombination of I_2 in rare-gas complexes has been reviewed by Roncero *et al*.[8] Recent real-time pump−probe experiments of $I_2(Ar)_n$[6,9,10] in combination with molecular dynamics simulations,[7] and of mass-selected ionic $I_2^-(Ar)_n$ clusters,[11−13] have been performed on the femto- or picosecond time scale, and they have provided a detailed microscopic picture of the caging process. Furthermore, the dependence of the fragment kinetic energy and angular distribution on the size of the cluster cage has also been studied by classical trajectory calculations for the photolysis of HF in Ar clusters.[14]

Of higher complexity is the study of chemical reactions induced by photodissociation of a chromophore molecule in a molecular cluster. In this context, the groups of Soep[15,16] and Wittig[1,17] are mentioned who have pioneered the method of aligning bimolecular collision partners in small van der Waals complexes by photoexcitation of a complex bound atom[15,16] or molecule.[1,17] Concerning our present cluster work we refer especially to the photolysis results on homogeneous $(OCS)_n$ clusters where the formation of the product S_2 was found to arise from the reaction of a primary sulfur atom fragment with OCS cage molecules.[18] In addition to S_2, vibrationally, rotationally, and translationally cold CO products were also detected but only if the cluster size exceeded five OCS molecules. The photodissociation of small clusters of HI[19−22] and CH_3I[23−29] was studied by time-of-flight,[20−22,26−29] REMPI,[19] LIF,[24,25] or Raman[23] detection of the products and/or of their energy distributions. For both these systems the formation of I_2 was observed and evidence was presented that this product is not only created in small clusters but even in dimers. I atom detection recently revealed a relaxation of the translational energy and the anisotropy parameter β compared to monomer photodissociation.[21,27−29] These results were discussed in terms of caging of the I atoms that may either react in or escape from the cluster. However, the mechanism of I_2 formation in the cluster is still a matter of uncertainty as also concerted photolytic mechanisms are under discussion for both systems.[22−25,29,30] Furthermore, in the case of $(HI)_n$ cluster photodissociation the H-atom flight time distribution was also investigated,[21,22] leading to features which were explained by elastic and inelastic H atom collisions involving the excitation of internal modes in HI cage species.

With the present work we extend our study on the photodissociation of homogeneous molecular clusters of nitrites $[RONO]_n$ with R being CH_3 and $C(CH_3)_3$.[31,32] Previously we were mainly concerned with small clusters ($\langle n \rangle \sim 20$), their formation conditions, and their effect on the NO fragment state distributions and alignments. The present study deals with larger clusters ($n > 400$) and focuses on reactions within the solvent cage. After S_1 photolysis of a methyl nitrite molecule weakly bonded in $[CH_3ONO]_n$, we detected by the LIF method nitroxyl HNO($\tilde{X}^1A'$) and formaldehyde $H_2CO(\tilde{X}^1A_1)$ in addition to rotationally cold and "hot" NO fragments. It is shown that following the primary dissociation step which yields NO($\tilde{X}^2\Pi$) and $CH_3O(\tilde{X}^2E)$, the disproportionation reaction of these radicals, mediated by the cluster "solvent" cage, proceeds to HNO and H_2CO.

[⊗] Abstract published in *Advance ACS Abstracts,* December 15, 1996.

S1089-5639(96)02507-8 CCC: $14.00

2. Experimental Section

A pulsed supersonic cluster beam was generated by expanding a mixture of methyl nitrite CH_3ONO ($\leq$6%) in Ar or He at backing pressures up to $p_0 = 4$ bar through a piezoelectric pulsed valve into a chamber equipped with a diffusion pump (700 L/s). Formation and growth of clusters, generally favored by increasing p_0, decreasing source temperature, and increasing nozzle diameter,[33−36] is decisively influenced by the nozzle geometry.[34−41] Thus, to obtain high centerline intensities and cluster sizes, we used a conical nozzle with an aperture d = 0.3 mm, a length of 14 mm, and an opening angle $2\theta = 14°$.

An excimer laser (Lambda Physik EMG 101 MSC) with an output at 308 nm and a repetition rate of ~10 Hz pumped two dye lasers simultaneously. A homemade Hänsch type dye laser (ASE < 5%) was used with various dyes (QUI, TMI, PQP, DMQ, and RDC 360) to photolyze the clusters. The second dye laser (Lambda Physik FL 2002 E) probed the photofragment NO($\tilde{X}^2\Pi$) and the cluster reaction products HNO($\tilde{X}^1A'$) and H_2CO($\tilde{X}^1A_1$) by the LIF technique. The NO fragments in the vibrational ground state were detected by 2+1 LIF,[42] using the NO[$\tilde{A}^2\Sigma^+(v'=0)\leftarrow\tilde{X}^2\Pi(v''=0)$] excitation step by operating the probe laser with the dye Coumarin 2. The HNO product was detected by its fluorescence excitation spectrum of the (010)−(000) vibronic band of the $\tilde{A}^1A'' \leftarrow \tilde{X}^1A'$ transition[43−48] using the dye Pyridine 1. The 0_0^0 and 4_0^1 vibronic bands of the $\tilde{A}^1A_2 \leftarrow \tilde{X}^1A_1$ band system in H_2CO[49−53] were measured analogously by employing the probe laser with the dye BMQ. Both lasers were linearly polarized to better than 97%. The counterpropagating dissociation and probe laser beams were crossed at an angle of 2° about 30 nozzle diameters from the pulsed piezoelectric valve; between the two laser pulses we chose an optical delay of ≈20 ns. The laser-induced fluorescence was collected by an unpolarized detector positioned at right angles to the plane defined by the two laser beams. Fluorescence detection of NO was achieved with a Hamamatsu R166UH PMT equipped with a solar blind filter (Corion), while for the H_2CO or HNO detection a Hamamatsu R928 PMT equipped with appropriate cutoff filters was used. The photomultiplier signals were amplified by a preamplifier and integrated by a digital boxcar integrator (SR 250). Photodiodes (Hamamatsu S1227BQ and Hamamatsu S1133-03) monitored the power of the dye lasers to normalize the measured LIF intensities and to correct for shot to shot fluctuations. A computer controlled the data acquisition, the variation of the backing pressure, and the tuning of the lasers. Methyl nitrite was prepared according to a published procedure[54] and purified by trap-to-trap distillation using IR and UV spectroscopy to check the purity.

3. Results

3.1. Detection of the NO Photofragment. The rotational-state distributions of the NO($\tilde{X}^2\Pi$) fragment after S_1 photolysis of the methyl nitrite monomer CH_3ONO and its clusters $[CH_3ONO]_n$ at ≈ 365 nm have previously been reported[31] for the four spin and Λ-doublet sublevels $F_1(A',A'')$ and $F_2(A',A'')$ in the NO vibrational states $v'' = 0$ and 1. For the NO vibrational state $v'' = 0$ the monomer photodissociation yielded a Gaussian-shaped rotational-state distribution covering $J'' = 20.5-50.5$ with a maximum around $\langle J''\rangle = 35.5$. As the molecular beam source and the expansion conditions differ from our earlier studies, a reinvestigation became necessary. Figure 1a shows the rotational-state distributions of the four sublevels of NO after excitation of the methyl nitrite chromophore in a cluster formed in an Ar expansion ($p_0 = 4$ bar, CH_3ONO partial pressure 240 mbar). Excitation at $\lambda = 365$ nm occurred into the quasibound

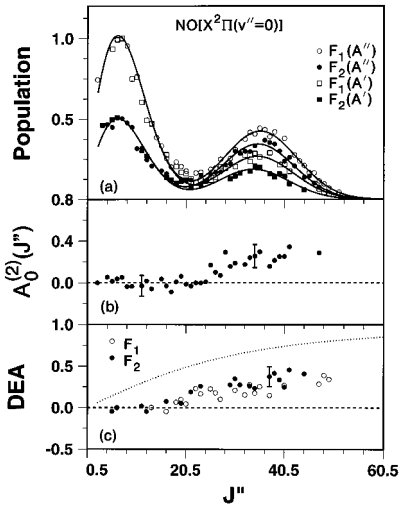

Figure 1. Scalar and vectorial properties of the NO($v''=0$) fragments emerging from the photodissociation of $[CH_3ONO]_n$ clusters formed in an expansion with Ar at a total backing pressure $p_0 = 4$ bar and a methyl nitrite partial pressure of 240 mbar. The cluster-bound CH_3ONO chromophore was excited to $S_1(n^* = 1)$ at 365 nm: (a) Rotational-state populations of the four sublevels $F_1(A',A'')$ and $F_2(A',A'')$ of NO($\tilde{X}^2\Pi, v''=0$). (b) Rotational alignment $A_0^{(2)}$ of the NO fragment as a function of the rotational state J''. (c) Degree of electron alignment (DEA) of the two spin−orbit states F_1 and F_2 of NO($\tilde{X}^2\Pi, v''=0$). The dotted line describes the maximum value for a planar dissociation of an isolated CH_3ONO. The error bar indicates one standard deviation.

state $n^* = 1$ which corresponds to one quantum of the N═O stretching mode v_3 in the $S_1(n\pi^*)$ state of CH_3ONO. A *bimodal* rotational distribution was obtained, similar to previous experiments[31] and analogous investigations of the *tert*-butyl nitrite monomer $(CH_3)_3CONO$ and its clusters $[(CH_3)_3CONO]_n$.[32]

The cold J'' distribution, extending up to $J'' \approx 20.5$, is exclusively due to NO($\tilde{X}^2\Pi$) fragments from cluster photodissociation and follows a Boltzmann distribution with a temperature $T_{rot} \approx 250 \pm 50$ K for all sublevels. The two almost degenerate Λ-doublet states A' and A'' in each of the two spin states F_1 and F_2 are equally populated, so that the degree of electron alignment (DEA) is zero for low J'' values (Figure 1c). The DEA reflects the orientation of the unpaired pπ electron with respect to the plane of rotation.[55,56] Below the high J'' limit, mixing of the Λ-doublet states leads to a reduction of the maximum DEA value (±1), which is indicated by the dotted line in Figure 1c. The symmetry of the S_1 excited state of methyl nitrite with respect to the molecular plane is A'' so that the previously established planar fragmentation[57−62] should lead to a clear propensity for the same symmetry A'' in the NO($\tilde{X}^2\Pi$) fragment. The observed value of DEA = 0 implies that any vestige of the electronic state of the parent molecule before fragmentation has been lost under cluster conditions. The rotational alignment $A_0^{(2)}$ is a measure of the correlation between the transition dipole moment $\boldsymbol{\mu}$ of the parent molecule and the angular momentum $\boldsymbol{J}$ of the NO fragment.[42,63] The dipole moment $\boldsymbol{\mu}$ of the $S_1 \leftarrow S_0$ transition is perpendicular to the plane of the CH_3ONO molecule with respect to the O−N═O moiety.[64] Consequently a planar fragmentation implies $\boldsymbol{J}\|\boldsymbol{\mu}$ which gives rise to $A_0^{(2)} = 0.8$. A reduction of this limiting value can be caused either by out of plane rotations of the parent molecule due to a long lifetime or by deviations from the planarity of the fragmentation process. The rotational alignment $A_0^{(2)}$ measured in this work using the same procedure as reported in previous publications[42,63] is shown in Figure 1b. For the low J'' distribution $A_0^{(2)}$ is zero, indicating that the ($\boldsymbol{\mu}$,$\boldsymbol{J}$) vector correlation has been completely lost which follows the

TABLE 1: Comparison of the Scalar and Vectorial Properties of the "Hot" ($J'' > 20.5$) Rotational-State Distributions of the NO($\tilde{X}^2\Pi, v''=0$) Photofragments Emerging from the Photodissociation of CH_3ONO and $[CH_3ONO]_n$ at ≈ 365 nm

	monomer	cluster	error
$\langle J'' \rangle$	35.5	35.5	±1
$\Delta J''_{fwhm}$	13	17	±1
P_{rot}			±5%
$F_1(A'')$	0.41	0.35	
$F_1(A')$	0.17	0.22	
$F_2(A'')$	0.31	0.28	
$F_2(A')$	0.11	0.15	
F_1/F_2 (tot)	1.40	1.30	±5%
F_1/F_2 (A'')	1.30	1.25	±5%
F_1/F_2 (A')	1.60	1.45	±5%
DEA (tot)	0.44	0.26	±5%
DEA (F_1)	0.41	0.23	±5%
DEA (F_2)	0.48	0.30	±5%
$A_0^{(2)}$	0.46	0.24	±0.05
fraction of "hot" NO	100%	39 ± 10%	

behavior of the DEA. A strong preference for the spin state F_1 lying 123.14 cm^{-1} below F_2[65] was observed for the cold J'' distribution: $P(F_1)/P(F_2) \approx 2$ corresponds to a spin Boltzmann temperature of ≈250 K which is in excellent agreement with the observed rotational temperature.

The results for the higher rotational-state distribution showing J'' values between 20.5 and 54.5 are summarized in Table 1 and compared to the corresponding results of the pure monomer photodissociation. The Gaussian distribution is centered at $\langle J'' \rangle = 35.5$ with $\Delta J''_{fwhm} \approx 17$, and is thus similar to the rotational-state distribution observed for methyl nitrite monomer dissociation except for a slight broadening. That this broadening is due to cluster photodissociation is supported by the reduction of the rotational alignment from $A_0^{(2)} \approx 0.46$ to ≈ 0.24 for the monomer and the present case (Figure 1b), respectively. The complementing DEA vector correlation is depicted in Figure 1c. Consistent with the $A_0^{(2)}$ reduction, it is reduced from 0.44 for the monomer to 0.26 for the cluster photodissociation. These results show a strong resemblance to the *tert*-butyl nitrite experiments[32] and parallel the previous experimental findings on methyl nitrite monomers and clusters.[31] The main difference is a considerably enhanced clustering under the present experimental conditions, manifested by a much greater percentage of rotationally relaxed NO fragments and an increased reduction of the vector correlations $A_0^{(2)}$ and DEA. The higher backing pressure, and a nozzle geometry favoring cluster formation, lead to this desired effect.

3.2. Fluorescence Excitation Spectra of H_2CO and HNO. Besides the NO($\tilde{X}^2\Pi$) fragment, we detected also formaldehyde and nitroxyl products from cluster photolysis. Using LIF spectroscopy after selective S_1 photodissociation of cluster-bound CH_3ONO from the state $n^* = 1$ at 365 nm, the product $H_2CO(\tilde{X}^1A_1)$ was identified by the fluorescence excitation spectrum of the 0_0^0 and 4_0^1 vibronic bands of the $\tilde{A}^1A_2 \leftarrow \tilde{X}^1A_1$ electronic transition. The 0−0 transition is electric-dipole forbidden, but magnetic-dipole allowed.[49,65] The LIF spectrum shown in Figure 2a was recorded in a beam consisting of Ar as carrier gas at $p_0 = 4$ bar with a partial methyl nitrite pressure of 240 mbar. Figure 2b displays the calculated rotational spectrum which is based on an asymmetric rotor by adopting the spectroscopic constants from Clouthier and Ramsay;[49] the population distribution of the ortho−para nuclear hyperfine states provided by the best fit corresponded to room temperature.

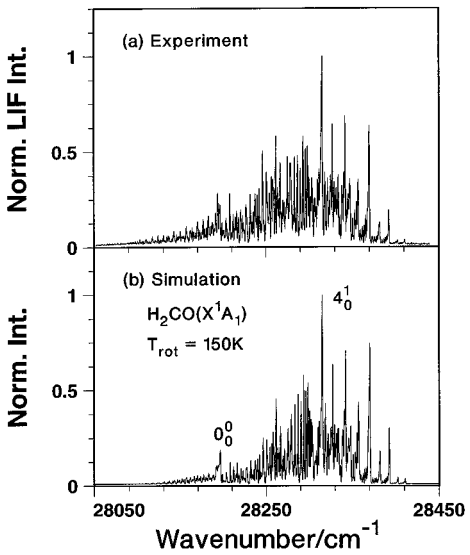

Figure 2. (a) Fluorescence excitation spectrum of $H_2CO(\tilde{X}^1A_1)$ measured after S_1 photodissociation of cluster-bound CH_3ONO at 365 nm. Methyl nitrite with a partial pressure of 240 mbar was expanded in argon at a total stagnation pressure $p_0 = 4$ bar. (b) Calculated spectrum of the 0_0^0 and the 4_0^1 bands of formaldehyde, assuming a Boltzmann distribution for the rotational state population with $T_{rot} = 150$ K.

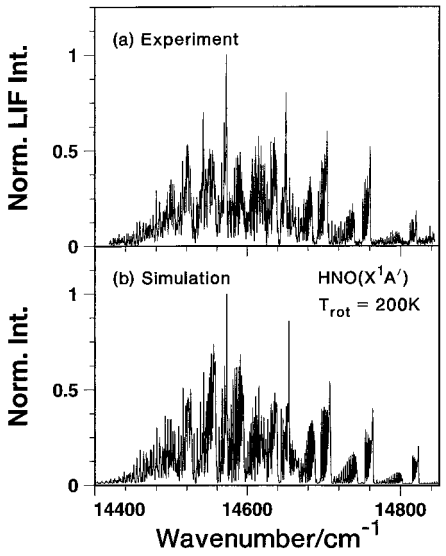

Figure 3. (a) Fluorescence excitation spectrum of $HNO(\tilde{X}^1A')$ recorded after S_1 photodissociation of cluster-bound CH_3ONO at 365 nm. The experimental conditions were as described in Figure 1 and 2 for the detection of NO and H_2CO. (b) Calculated spectrum of the (010)−(000) absorption of $HNO(\tilde{X}^1A')$, assuming a Boltzmann distribution of the rotational state population with $T_{rot} = 200$ K.

Although an exact matching of the intensities of the calculated and the measured fluorescence excitation spectrum would also require a correction for the rotational-state-dependent emission lifetime,[52,53] we obtained a satisfactory agreement by assuming a Boltzmann distribution with a temperature of 150 K for the rotational-state population.

The product HNO is a chemically unstable intermediate with a room temperature lifetime estimated to be 1−40 s.[66,67] Our measured HNO fluorescence excitation spectrum of the (010)−(000) vibronic band of the $\tilde{A}^1A'' \leftarrow \tilde{X}^1A'$ transition[43−48] is shown in Figure 3a; it has been recorded under the same conditions as formaldehyde given above. Figure 3b depicts the calculated spectrum obtained with the same asymmetric rotor program as applied for H_2CO using the rotational constants

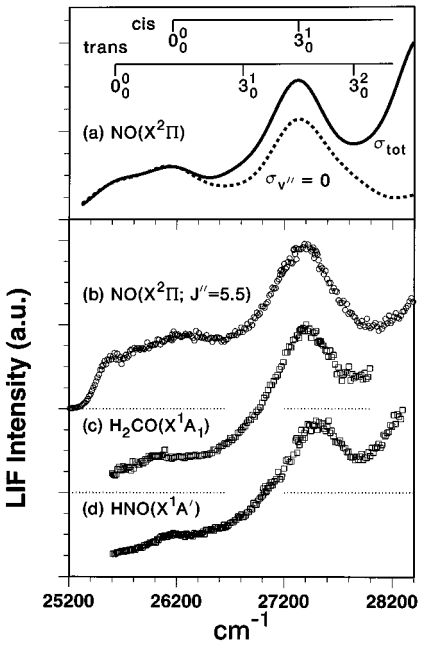

Figure 4. Photoproduct yield spectra: (a) The broken line shows the partial cross section $\sigma(\tilde{\nu};v''=0)$ of the $S_1 \leftarrow S_0$ transition of CH_3ONO recorded by monitoring the NO($\tilde{X}^2\Pi$) fragment from a pure monomer photodissociation. Summation of the partial cross sections $\sigma(\tilde{\nu},v'')$ for the NO fragment vibrational states $v'' = 0$, 1, and 2 ($\tilde{\nu}$ < 28 400 cm^{-1}) yields the total cross section $\sigma_{tot}(\tilde{\nu})$. The assignment for the ν_3 progression of the cis and trans conformer of methyl nitrite is given on top of the panel. (b) Cluster partial cross section $\sigma(\tilde{\nu};v''=0)$ obtained by monitoring cold NO($\tilde{X}^2\Pi$;J''=5.5). (c) Photoproduct yield spectrum for the vibrational ground state of $H_2CO(\tilde{X}^1A_1)$ formed in the photodissociation of $[CH_3ONO]_n$ clusters. (d) Photoproduct yield spectrum for the vibrational ground state of HNO($\tilde{X}^1A'$) emerging from the photodissociation of cluster-bound CH_3ONO.

reported by Dixon *et al.*[48] and Petersen *et al.*[68] for the excited and the ground state. A Boltzmann population distribution with a temperature of 200 K provided the best fit to the rotational intensities of the measured fluorescence excitation spectrum.

3.3. Cluster Product Yield Excitation Spectra. The broad vibronic features of the CH_3ONO $S_1 \leftarrow S_0$ absorption have been assigned to a progression of the N═O stretching mode ($3_0^{n^*}$) with two overlapping band systems due to the cis and trans rotamer[64] (see Figure 4a). *trans*-CH_3ONO is less stable than the cis conformer by 3.5 ± 0.2 kJ/mol;[69] giving rise to a preferred population of the cis form at room temperature and a similar preference in the supersonic jet assuming "sudden freezing".[70] Indeed, the dominance of *cis*-CH_3ONO is indicated by the total absorption cross section $\sigma_{tot}(\tilde{\nu})$ for the pure monomer, which has been reported previously.[71] Because the photofragment yield spectrum (PHOFRY) was found to be independent of the NO($\tilde{X}^2\Pi$) rotational state within the experimental error, summation of the appropriately weighted PHOFRY spectra for the NO vibrational levels $v'' = 0$, 1, and 2, provides the low-energy part of the absorption spectrum given by $\sigma_{tot}(\tilde{\nu}) = \sum_{v''}\sigma(\tilde{\nu};v'')$. This is depicted in Figure 4a together with the NO($\tilde{X}^2\Pi$,v''=0) PHOFRY spectrum[71] recorded by monitoring NO in $J'' = 36.5$.

The corresponding PHOFRY spectrum of the clusters $[CH_3ONO]_n$, shown in Figure 4b, has been measured by monitoring a low rotational state ($J'' = 5.5$) of NO($\tilde{X}^2\Pi$,v''=0), which stems exclusively from cluster photodissociation. The monomer and cluster partial cross sections $\sigma(\tilde{\nu};v''=0)$ obtained in this manner, parallel each other except for a broadening of the vibronic resonances in the latter and small differences in the fragment vibrational state distribution as has also been found previously for *tert*-butyl nitrite.[32]

Product excitation yield spectra of $[CH_3ONO]_n$ clusters were recorded by scanning the excitation (dissociation) wavelength between 25 600 and 28 400 cm^{-1} while monitoring the vibrational ground state of $H_2CO(\tilde{X}^1A_1)$ and HNO($\tilde{X}^1A'$) by 1+1 LIF spectroscopy. These excitation yield spectra of the cluster photoproducts formaldehyde and nitroxyl shown in Figure 4, parts c and d, are similar to the cluster PHOFRY spectrum in Figure 4b. The features reflect the n^* vibronic band progression of the $S_1 \leftarrow S_0$ methyl nitrite absorption; they are also broadened but slightly different in their contributions compared to $\sigma(\tilde{\nu};v''=0)$ of NO($\tilde{X}^2\Pi$) (see discussion).

3.4. Pressure Dependence of Cluster Formation. If pure Ar is expanded under the present stagnation conditions (see section 3.2) the formation of Ar_m clusters is expected. From the kinetics of cluster formation in a supersonic beam expansion[72] it is therefore conceivable that mixed heterogeneous clusters $Ar_m[CH_3ONO]_n$ clusters are also formed initially during the condensation process. However, due to the difference in condensation energy between the argon carrier (≈80−100 cm^{-1})[73−75] and the CH_3ONO seed (300−700 cm^{-1}, depending on the configuration of the *cis*-CH_3ONO dimer as calculated using the Gaussian 92 program system with the G-31G* basis set), the survival of such mixed clusters beyond the nozzle is unlikely and we therefore assume that homogeneous $[CH_3ONO]_n$ clusters or clusters of CH_3ONO with only a few Ar incorporated are the dominating species in the beam. This is consistent with the previous mass spectrometric analysis of methyl nitrite and *tert*-butyl nitrite clusters.[31]

When the backing pressure p_0 of the mixture of carrier gas and CH_3ONO is increased from 0.1 to 3 bar, the process of CH_3ONO cluster formation can be followed. Monitoring the yield of rotationally cold NO($\tilde{X}^2\Pi$;J''=5.5) fragments produced exclusively from cluster photolysis, the cluster formation is revealed as a phase transition.[76−79] If H_2CO and HNO are also products which are formed solely by clusters, their yield dependence on p_0 should parallel the cluster formation process. To confirm this expectation we measured the intensity of the LIF signal from $H_2CO(\tilde{X}^1A_1)$ and HNO($\tilde{X}^1A'$) which is proportional to the production yield of these species. Figure 5 shows the LIF intensity versus p_0 in the pressure range $0 \le p_0 \le 3$ bar keeping the CH_3ONO concentration in Ar and He constant at 6%. The intensities are corrected (normalized) for the density and the velocity of the beam which are known to change with p_0.[80] In the case of He (Figure 5b) the LIF signal intensities for the three investigated product species show the same dependence on p_0. They are zero below a stagnation pressure of ∼0.5 bar and then abruptly rise to a maximum within a pressure range of ≈0.7 bar. This observation implies that formaldehyde and nitroxyl must be products resulting from the photolysis of methyl nitrite in a cluster environment and not from CH_3ONO monomer dissociation. Analogous pressure dependences for cluster formation in supersonic beams have been reported using other detection techniques[81,82] and more recently we observed this phase transition also for $(CH_3)_3CONO$.[32] A similar p_0 dependence of the LIF signal intensities of NO($\tilde{X}^1\Pi$) and $H_2CO(\tilde{X}^1A_1)$ is observed with the carrier gas Ar (Figure 5a), for which the pressure axis has been scaled by a factor of 3, because of the greater collision cross section for energy transfer of Ar compared to He. Cluster formation starts here at $p_0 \sim 0.15$ bar and reaches the maximum within about 0.5 bar.

Cluster growth in the supersonic expansion can alternatively be followed by increasing the CH_3ONO partial pressure between

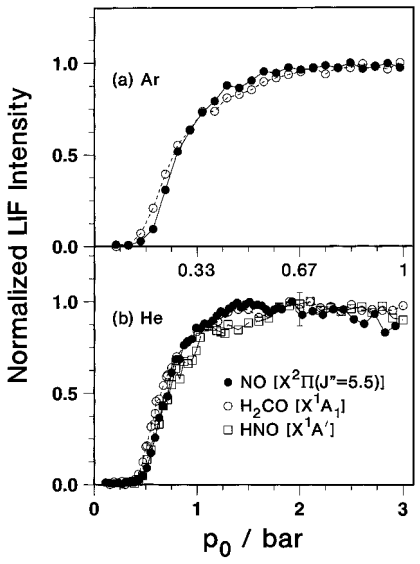

Figure 5. Cluster formation as a function of the backing pressure p_0 in a supersonic beam expansion of methyl nitrite (6%) in (a) Ar and (b) He. The data points show the normalized LIF signal intensities measured for NO($\tilde{X}^2\Pi;v''=0;J''=5.5$) cluster photofragments, and for the cluster photoproducts $H_2CO(\tilde{X}^1A_1)$ and $HNO(\tilde{X}^1A')$ in their vibrational ground state. Cluster bound CH_3ONO was excited at 365 nm. The error bar indicates one standard deviation.

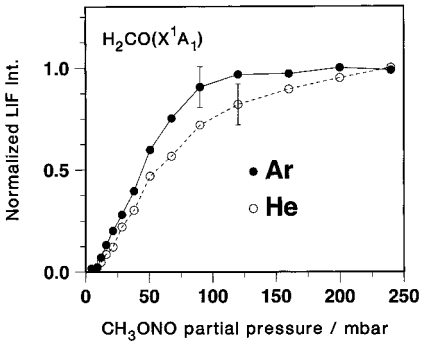

Figure 6. Cluster formation as a function of the partial pressure of CH_3ONO in Ar and He at a fixed backing pressure $p_0 = 4$ bar. The LIF signal of the vibrationless $H_2CO(X^1A_1)$ was measured after photodissociation of cluster-bound CH_3ONO at 365 nm. The error bar indicates one standard deviation.

4 and 240 mbar, while keeping the total backing pressure constant ($p_0 = 4$ bar). The cluster size and cluster density in the beam increase with the methyl nitrite partial pressure up to a maximum where it levels off. The results obtained for the dependence of the $H_2CO(\tilde{X}^1A_1)$ LIF signal intensity on the methyl nitrite partial pressure in Ar and He are shown in Figure 6. Within experimental error they agree with each other and are similar to the p_0 dependences of the yield of the three product species depicted in Figure 5. The signal is zero below a CH_3ONO partial pressure of ~10 mbar and rises with increasing partial pressure to a maximum which is probably determined by the limited cooling effect of the carrier gas caused by saturation of the condensable species CH_3ONO in the gas mixture.[83−85] Similar dependences on the partial pressure have recently been observed for large homogeneous $(SF_6)_n$ clusters ($n = 100-3000$) using electron diffraction.[85]

4. Discussion

4.1. Cluster Photodissociation. The first part of the discussion deals with the photodissociation of methyl nitrite clusters which proceeds to the primary products NO and CH_3O. Some of these findings, although obtained for smaller cluster sizes, have been reported previously,[31] and are therefore discussed only briefly. On the basis of these results we discuss in the second part the bimolecular reaction of the primary products in the cluster cage.

The photodissociation process of methyl nitrite clusters excited to $n^* = 1$ at 365 nm was monitored by the rotational state distribution, the rotational alignment $A_0^{(2)}$, and the degree of electron alignment DEA of the NO($\tilde{X}^2\Pi,v''=0$) product. The results are shown in Figure 1 and summarized in Table 1 together with the corresponding monomer results found previously.[31] As has been discussed in our preceding papers,[31,32] the two different rotational distributions (Figure 1a) are created by the photodissociation of methyl nitrite in different cluster environments. The cold NO fragments stem from nitrite molecules for which their O−N═O chromophore is "solvated" in the cluster. The ejected NO is thus thermalized by the cluster environment which causes a cold rotational-state distribution, a low translational energy, and the destruction of the alignments $A_0^{(2)}$ and DEA. On the other hand the rotationally "hot" and aligned NO fragments arise from the photodissociation of methyl nitrite molecules with a free uncomplexed chromophore located on the cluster surface. Related results have recently been reported for the photolysis of methyl nitrite on a dielectric surface. Simpson and co-workers[86] found that the slow-moving NO fragments ejected from surface molecules have Boltzmann rotational-state distributions and that their rotational temperature rises with the translational energy of the detected NO. The fragments with a very high velocity assumed a Gaussian shaped rotational-state distribution.

The detection of $[CH_3ONO]_n$ cluster properties could be achieved by probing cold NO($v''=0,J''=5.5$) fragments as has been demonstrated for $(CH_3)_3CONO$.[32] In this manner we measured the cluster partial cross section $\sigma(\tilde{\nu};v''=0)$ depicted in Figure 4b. Compared to the corresponding monomer cross section shown in Figure 4a, the vibrational resonances n^* of the $S_1 \leftarrow S_0$ absorption are broadened, i.e. the vibrational energy distribution of the NO fragments is slightly changed, presumably due to the interaction of the CH_3ONO molecule with the cluster environment. Furthermore, cluster probing by means of a low rotational J'' state also made it possible to follow the formation of $[CH_3ONO]_n$ as a function of the backing pressure p_0, providing the phase-transition curve in Figure 5. This curve describes how the number of CH_3ONO molecules weakly bound in clusters increases relative to the total number of CH_3ONO molecules present in the beam with the backing pressure. As long as p_0 is too low for the formation of clusters, this ratio is zero. When clustering starts, it increases very rapidly with p_0, leading eventually to a situation where all the methyl nitrite molecules seeded in the carrier gas are cluster bound. Changing from the carrier gas He to Ar, while the source temperature, the nozzle geometry, and the CH_3ONO concentration were kept constant, the size distribution of the clusters was changed. The larger collision cross section of Ar compared to He in the adiabatic expansion process shifts the phase transition to lower p_0 by a factor of ≈3. This is in agreement with the result found for *tert*-butyl nitrite[32] and compares favorably with the ratio of the collision cross sections of the two carrier gases.[87]

A rough estimate of the average cluster size in our experiment may be obtained by the concept of corresponding beams evaluated by Hagena.[33−36,39,40,88] Within this description the average cluster size $\bar{n}$ is a function of the condensation parameter Γ^* which, in turn, is a function of p_0 (in mbar), the nozzle diameter d (in μm), and the source temperature T_0 (in K). In the case of Ar one obtains the expression[33,40]

$$\Gamma^* = 1646 p_0 d^{0.5} T_0^{-2.2875} \quad (1)$$

For a conical nozzle, d has to be replaced by $d_{equ} = 0.737d/\tan\theta$, where 2θ is the opening angle.[39,40,88] From scattering experiments between He and Ar_n, Buck and Krohne[88] have derived the following relationship for $\bar{n}$ and Γ^*

$$\bar{n} = 38.4(\Gamma^*/1000)^{1.64} \quad (2)$$

applicable to cluster sizes up to $\bar{n} \leq 400$. Since the binding energy of the *cis*-methyl nitrite dimer was calculated to be between 300 and 700 cm^{-1} depending on the configuration (see section 3.4), and is thus greater than the Ar−Ar interaction of about 80−100 cm^{-1},[73−75] cluster formation should be stronger and consequently eq 2 will merely provide a lower limit for the average cluster size. According to Figure 5, the onset of clustering was observed at $p_0 \approx 150$ mbar, which corresponds to $\bar{n} > 5$. A constant density of cluster-bound CH_3ONO is reached at ≈0.7 bar which yields $\bar{n} > 60$. With the applied backing pressure of 4 bar, however, the condensation parameter Γ^* becomes so large that eq 2 is no longer valid and only a lower limit for the average cluster size $\bar{n} > 400$ can be given. An upper limit for the average cluster size may be estimated from the ratio of molecules which are located on the cluster surface to all cluster components. For sufficiently large clusters $\bar{n} > 100$ the fraction of surface molecules F is related to the cluster size by $\bar{n} = (4/F)^3$.[89] The high J'' Gaussian rotational-state distribution of the NO($\tilde{X}^2\Pi$) photofragments has been attributed to the photodissociation of CH_3ONO molecules located on the cluster surface. It represents a fraction of ≈40% of the total population obtained by integration over the low J'' Boltzmann and the high J'' Gaussian profiles (see Figure 1a and Table 1). Assuming that the photodissociation of all surface-bound CH_3ONO molecules leads to rotationally hot NO fragments, we find an upper limit of $\bar{n} = 1000$ for the average cluster size in an Ar expansion at $p_0 = 4$ bar. Such clusters possess a diameter of approximately 4.5 nm if a *cis*-CH_3ONO diameter $d \approx 4.5$ Å[90,91] is adopted. From these considerations we then cautiously suggest that the average methyl nitrite clusters created in our experiment consist of 400−1000 molecules at $p_0 = 4$ bar.

4.2. Photoinduced Bimolecular Reactions in the Cluster. *Determination of the Reaction Products.* Besides NO($\tilde{X}^2\Pi$), formaldehyde $H_2CO(\tilde{X}^1A_1)$ and nitroxyl HNO($\tilde{X}^1A'$) have been detected as products resulting from $[CH_3ONO]_n$ cluster S_1 photodissociation. Both products were identified by measuring the fluorescence excitation spectra depicted in Figures 2a and 3a. Under the assumption that the rotational-state population follows a Boltzmann distribution, the simulation spectra of Figures 2b and 3b reproduce the excitation spectra with rotational temperatures of 150 and 200 K, respectively.

By scanning the dissociation wavelength while monitoring the vibrational ground states of $H_2CO(\tilde{X}^1A_1)$ and HNO($\tilde{X}^1A'$) using LIF spectroscopy, the yield excitation spectra of the two reaction products (Figure 4, part c and d, respectively) have been obtained. They are similar to the yield spectrum of the cluster photofragment NO($\tilde{X}^2\Pi$,v''=0,J''=5.5) of Figure 4b and also show a similar broadening of the vibrational resonances when compared to the corresponding monomer spectrum (Figure 4a). The origin of H_2CO and HNO is therefore indicated to be the same species as that for rotationally cold NO. Since HNO($\tilde{X}^1A'$) and $H_2CO(\tilde{X}^1A_1)$ are the products of the bimolecular reaction between the primary photofragments NO and CH_3O (vide infra) their slightly different $\sigma(\tilde{\nu};v''=0)$ spectra compared to that monitoring rotationally cold NO($\tilde{X}^2\Pi$) could be due to a small dependence of the HNO($\tilde{X}^1A'$) and $H_2CO(\tilde{X}^1A_1)$ formation on the initial vibrational excitation of the NO reactant.

The pressure dependence of the LIF signal intensities measured for the H_2CO and HNO photoproducts, shown in Figure 5, closely follows that of the rotationally cold NO-(v''=0,J''=5.5) fragments. As the cold NO can only be produced from dissociation of CH_3ONO embedded in the cluster,[31] this observation, as well as the yield excitation spectra discussed above, demonstrate that formaldehyde and nitroxyl must be products of methyl nitrite photolysis in a cluster environment; they are clearly not primary products of the CH_3-ONO monomer photodissociation. Moreover this conclusion is also corroborated by the findings of Figure 6 where the dependence of the $H_2CO(\tilde{X}^1A_1)$ LIF signal intensity on the CH_3-ONO partial pressure at constant p_0 parallels the cluster formation as a function of p_0 shown in Figure 5.

The Reaction Mechanism. Having identified the products HNO and H_2CO as originating from photodissociation of methyl nitrite in a cluster environment, we proceed to elucidate the underlying mechanism. Under *isolated molecule conditions* the primary step of the photodissociation has been established to be exclusively:[31,59,92−94]

$$CH_3ONO \xrightarrow{h\nu} CH_3O + NO \quad (3)$$

Particularly relevant to the present cluster findings appear the photolysis results in noble gas matrices. On the basis of a study by Brown and Pimentel[95] the groups of Huber[96−99] and Jacox[100] demonstrated that photolysis of isolated CH_3ONO in an Ar matrix at 365 nm produces exclusively HNO and H_2CO which form a hydrogen-bonded complex. The initially formed fragments NO and CH_3O are compelled by the rigid cage to recollide. This can lead to a competition between the recombination and the disproportionation reaction:

$$CH_3O + NO \rightarrow CH_3ONO \qquad \Delta H \approx -14\,600\ cm^{-1} \quad (4)$$

$$\rightarrow H_2CO + HNO \qquad \Delta H \approx -8800\ cm^{-1} \quad (5)$$

The primary fragments, being confined to the matrix cage, can react back to CH_3ONO which subsequently may be photolyzed again, or they can disproportionate to HNO and H_2CO which will undergo no further reaction when excitation occurs at 365 nm.

Several studies on the photolysis[101−107] of CH_3ONO in a static or in a flow cell have also reported the production of formaldehyde and nitroxyl besides NO and CH_3O. The existence of the disproportionation channel (eq 5) has further been established by investigations of the kinetics of the $CH_3O + NO$ reaction in the bulk gas phase.[108−111] Under these conditions, collisions between NO and CH_3O become much less probable so that the primary photofragments can easily be detected while the formation of HNO and H_2CO is less pronounced than in the matrix. Zellner[106] proposed that the photodissociation of CH_3ONO in the bulk gas phase proceeds at least in part directly to HNO and H_2CO as primary products but this is clearly contradicted by our observation that these products only emerge from cluster but not from monomer photodissociation. Evidence that the reaction 5 is the source of HNO and H_2CO formation was first been reported by Napier and Norrish[101] who observed a marked increase of the nitroxyl intensity in the presence of added NO. Sanders *et al.*[105] then provided compelling evidence by observing that in the presence of excess NO the LIF signal of HNO increased by a factor of about 10 and that the rise time

of the HNO LIF signal as a function of added NO parallels the disappearance rate of the CH_3O radical.

On the basis of these findings it appears straightforward to explain the formation of H_2CO and HNO in our cluster photodissociation experiments with the disproportionation reaction 5 between the primary photofragments mediated by a *cluster cage effect*. However, two further conceivable mechanisms for the product formation in the cluster environment may have to be considered. The first is concerned with the direct elimination of HNO from a cluster-bound CH_3ONO molecule

$$(CH_3ONO)_{cluster} \xrightarrow{h\nu} H_2CO + HNO \qquad (6)$$

while the second involves reactions of the primary fragments with CH_3ONO solvent molecules:

$$CH_3O + CH_3ONO \rightarrow CH_3OH + H_2CO + NO \qquad (7)$$

$$NO + CH_3ONO \rightarrow HNO + H_2CO + NO \qquad (8)$$

A direct, i.e. one-step fragmentation of CH_3ONO to $HNO(\tilde{X}^1A')$ and $H_2CO(\tilde{X}^1A_1)$ (eq 6), would, on symmetry and geometry grounds, only be possible if internal conversion to the ground state S_0 could occur. Only the S_0 dissociation of *trans*-methyl nitrite could yield $HNO(\tilde{X}^1A')$ and $H_2CO(\tilde{X}^1A_1)$ which would proceed via a (dynamically unfavorable) 4-center transition state[112,113] as has been proposed by Batt *et al.*[114] for the pyrolysis mechanism of methyl nitrite. However, it is experimentally and theoretically well established that the dissociation of CH_3ONO on the S_1 surface is very fast in the range of about 200 fs[57,59,115−119] and that the quantum yield for fragmentation to NO and CH_3O is one.[92,120] Thus $S_1 \rightarrow S_0$ internal conversion and hence reaction 6 can be ruled out. (In this context, it is noted that a reaction of electronically excited CH_3ONO (S_1) with a CH_3ONO (S_0) cluster molecule, yielding HNO and H_2CO as reactions products, is energetically not feasible.[121−124])

The reaction of methoxy with methyl nitrite (eq 7) proceeds through H abstraction followed by an exothermic ($\Delta H \approx -10\,400$ cm^{-1})[121,122] decomposition of the CH_2ONO radical according to $CH_2ONO \rightarrow H_2CO + NO$. Evidence for the reaction channel involving CH_2ONO formation has been obtained in studies of the reaction of O, H, F, Cl, and OH radicals with CH_3ONO.[125−128] Adopting Warneck's estimate of a C−H bond dissociation energy of ≈32 500 cm^{-1} for CH_3ONO,[126] the H-atom abstraction of CH_3ONO by CH_3O leading to CH_2ONO would be exothermic by ≈3800 cm^{-1}. However, in pyrolysis work,[129] the analogous hydrogen abstraction from CH_3ONO by ethoxy radicals was shown to be extremely slow and furthermore it was found that the reaction of C_2H_5O with NO is much more rapid than the ethoxyethyl nitrite reaction.[130] Therefore, assuming the reactivities of methoxy and ethoxy as being here roughly similar, we can conclude that the hydrogen abstraction (eq 7) is at most only of minor importance in our cluster experiments. Finally, in the reaction of NO with CH_3ONO (eq 8) the H-abstraction step is endothermic[121−124] by ≈16 000 cm^{-1} which greatly exceeds the NO available energy from the primary dissociation process of <8000 cm^{-1} when excitation at ∼365 nm is applied.[31,58]

Thus the mechanism explaining both, the formation of $HNO(\tilde{X}^1A')$ and $H_2CO(\tilde{X}^1A_1)$ following methyl nitrite photodissociation, is based on the disproportionation reaction of the primary fragments CH_3O and NO (eq 5) within the cluster cage. The reaction involves the abstraction of an H atom from CH_3O leading to H_2CO, which is expected to cause excitation of the out of plane bending vibration ν_4 due to the symmetry change from C_{3v} to C_{2v}. Indeed this mode was found to be excited. Generally, alkoxy radicals with at least one α H atom react with NO via the two competing routes recombination and disproportionation. The latter is known as an important step in the reduction of nitric oxide in the combustion of alkyl nitrates and nitrites, and it is of relevance to the atmospheric chemistry of CH_3O which is produced in the oxidation of CH_4.[131] The existence of this disproportionation reaction has been further confirmed in investigations on the reactions of the radicals ethoxy[109,132−135] and isopropoxy[136−138] with NO:

$$CH_3CH_2O + NO \rightarrow HNO + CH_3CHO \qquad (9)$$

$$(CH_3)_2CHO + NO \rightarrow HNO + (CH_3)_2CO \qquad (10)$$

Finally it is noted that in the context of the present study, we have also investigated the photodissociation of homogeneous ethyl nitrite clusters $[C_2H_5ONO]_n$. We found $HNO(\tilde{X}^1A')$ as a cluster reaction product analogous to $[CH_3ONO]_n$ which further corroborates the cluster cage mechanism leading via disproportionation to the formation of HNO.

In recent work the cage effect, relevant to the present study, has been shown to be especially effective in large clusters. The caging time scale ranges from femtoseconds to picoseconds, depending on the dissociation time as well as the size and temperature of the cluster.[7] Zewail and co-workers[6,9,10] reported the first direct observation of a caging process in real time studying the dissociation and recombination of iodine in argon clusters. Molecular dynamics calculations succeeded in reproducing these experimental results thus providing a microscopic picture of the process.[7] The caging was found to depend critically on the time scale of the dissociation of the guest molecule in the solvent cage. As mentioned above, the dissociation time of CH_3ONO on the S_1 surface lies in the range of ≈200 fs. This value is of the same order of magnitude as the dissociation time of I_2 in an $I_2{\cdot}Ar_n$ cluster excited to the directly dissociative $\tilde{A}$ state ($\tau_{diss} \approx 300$ fs) applied in the experiments of the Zewail group.[6,9,10] They observed a subsequent coherent recombination in an additional time span of 360 fs and furthermore complete caging in large clusters ($\bar{n} \geq 40$). In our cluster experiments the minimum time required for a recoil of the fragments from the solvating environment can be estimated if an axial elastic hard-sphere collision of the fragments with a rigid solvent cage is assumed. The distance between the fragments striking the cluster cage can be found from the optimized dimer structures (see section 3.4) and the velocity of the $NO(\tilde{X}^2\Pi, v''=0)$ and CH_3O fragments after photodissociation of CH_3ONO at ∼365 nm is known from Doppler profiles.[31] According to these data the minimum time for a reencounter of the photofragments is calculated to be >60 fs. The binding energy between the CH_3ONO molecules in the $[CH_3ONO]_n$ clusters is greater than that between the cage-forming Ar atoms (vide supra) in the $I_2{\cdot}Ar_n$ clusters investigated by Zewail and co-workers. Furthermore the mass of the cluster-forming constituents, the cluster size, and the speed of the fragments are greater in our experiment, making the cage effect even more favorable for an efficient recombination or disproportionation of the fragments. However, the energy transferred from the hot dissociation products CH_3O and NO to the solvent shell is expected to be high because the energy channeled into the degrees of freedom of these fragments amounts to about 14 000 cm^{-1} using excitation at 365 nm.[57,58] The kinetic energy is about 4500 cm^{-1} for each, NO and CH_3O[31,58] while the rotational energy is ∼2000 and 1100 cm^{-1} for NO and CH_3O, respectively.[58] Since the vibrational excitation of NO has previously been found to be almost unrelaxed by the cage effect,[31,32] we expect that a maximum energy of about 12 000

cm^{-1} is transferred to the cage. (It is noted that a conceivable contribution from the exothermicity of reactions 4 and 5 is here not included.) As our results indicated, this energy is sufficient to evaporate the cage, or at least part of it, to free cold NO, HNO, and H_2CO.

The cluster size dependence of photodissociation and recombination dynamics of the I_2^- chromophore in mass-selected $I_2^-(CO_2)_n$ clusters ($0 \leq n \leq 22$) has recently been investigated by Lineberger and co-workers[11−13] using picosecond laser pulses in conjunction with a tandem time-of-flight mass spectrometer. They observed no recombination for $n \leq 5$, a low recombination rate for $6 \leq n \leq 12$, a transition range $13 \leq n \leq 15$ in which the recombination rate rises markedly, and a much faster recombination for $n \geq 16$. As with the experiments of Zewail and co-workers the recombination yield increases with cluster size reaching complete recombination and a coherent I_2^- cage vibration in large clusters, for which at least one complete shell around the guest is accomplished. Therefore one might expect that complete caging and a fast recovery of the dissociating fragments in the photodissociation of $[CH_3ONO]_n$ clusters also requires at least one complete shell around the guest molecule. Assuming icosahedral packing, a complete shell around a single methyl nitrite molecule requires 12, the second shell an additional 42 molecules.[32] The cluster size dependence of the H_2CO and HNO product formation due to caging is reflected by the pressure dependences of the LIF signal intensities in Figure 5. Using the cluster size estimates derived in section 4.1, we find that H_2CO/HNO formation starts for $n > 5$ and reaches a maximum for $n > 60$. Thus our estimated lower bound for the cluster size is consistent with the size dependence found for the yield of caging and the rate of recombination by Lineberger and co-workers. The pressure curves shown in the Figures 5 and 6 reflect therefore not only the pressure dependence of cluster growth in the supersonic expansion but also the relative recombination or disproportionation yield of the caged primary photofragments as a function of the cluster size.

5. Conclusion

The photolysis of homogeneous methyl nitrite clusters $[CH_3ONO]_n$, where n is estimated to be 400−1000, proceeds along the primary step to $CH_3O(\tilde{X}^2E)$ and $NO(\tilde{X}^2\Pi)$. The NO product shows a bimodal (cold and "hot") rotational state distribution. The rotationally cold fragments ($J'' < 20.5$) have been thermalized by the cluster environment while the rotationally "hot" and aligned NO fragments stem from methyl nitrite molecules with a "free" chromophore located on the cluster surface. The distribution of the latter is similar to that found for NO which emerges from monomer photolysis. Since rotationally cold NO is produced only from clusters, its yield as a function of the backing pressure also reflects the cluster formation process. Besides NO and CH_3O, cluster photolysis furnishes the products $HNO(\tilde{X}^1A')$ and $H_2CO(\tilde{X}^1A_1)$. The dependence of their yields on the backing pressure follows closely the formation of cold NO and hence indicates that also HNO and H_2CO originate exclusively from cluster photolysis. The cluster cage effect is responsible for the formation of these products. Unless created from surface molecules, the "hot" primary fragments CH_3O and NO ($J'' = 20.5-50.5$) are temporarily trapped by the solvent cage where they collide with the molecules forming the cage and with each other giving rise to three competing processes: recombination to CH_3ONO, disproportionation to H_2CO and HNO, and thermalization with escape from the evaporating cluster cage. The cage evaporation originates from the transfer of up to 12 000 cm^{-1} of translational and rotational energy from the primary fragments to the solvent shell not including the contribution from the exothermicity of the reactions. The efficiency and the branching of the cage reactions leading to CH_3ONO, NO (cold), and HNO + H_2CO will depend on the size, binding energy, and temperature of the cluster. This was found to be consistent with the backing pressure dependences and the product yields of NO, HNO, and H_2CO.

Acknowledgment. Financial support of this work by the Schweizerischer Nationalfonds zur Förderung der wissenschaftlichen Forschung and the Alfred Werner Legat is gratefully acknowledged. We thank Dr. A. Furlan for helpful discussions, Dr. M. Rösslein for technical assistance, R. Pfister for synthesizing the relevant substances, and Dr. R. Carter for critically reading our manuscript.

References and Notes

(1) Shin, S. K.; Chen, Y.; Nickolaisen, S.; Sharpe, S. W.; Beaudet, R. A.; Wittig, C. *Adv. Photochem.* **1991**, *16*, 249.
(2) Castleman, A. W., Jr.; Wei, S. *Annu. Rev. Phys. Chem.* **1994**, *45*, 685.
(3) Gerber, R. B.; McCoy, A. B.; Garcia-Vela, A. *Annu. Rev. Phys. Chem.* **1994**, *45*, 275.
(4) Bernstein, E. R. *Annu. Rev. Phys. Chem.* **1995**, *46*, 197.
(5) Manz, J., Wöste, L., Eds. *Femtosecond Chemistry*; VCH: Weinheim, 1995; Vol. II., cluster articles therein.
(6) Wang, J.-K.; Liu, Q.; Zewail, A. H. *J. Phys. Chem.* **1995**, *99*, 11309.
(7) Liu, Q.; Wang, J-K.; Zewail, A. H. *J. Phys. Chem.* **1995**, *99*, 11321.
(8) Roncero, O.; Halberstadt, N.; Beswick, J. A. Caging and nonadiabatic electronic transitions in I_2-M complexes. In *Reaction Dynamics in Clusters and Condensed Phases*; Jortner, J., Ed.; Kluwer Academic Publishers: Netherlands, 1994; p 73.
(9) Potter, E. D.; Liu, Q.; Zewail, A. H. *Chem. Phys. Lett.* **1992**, *200*, 605.
(10) Liu, Q.; Wang, J.-K.; Zewail, A. H. *Nature* **1993**, *364*, 427.
(11) Papanikolas, J. M.; Gord, J. R.; Levinger, N. E.; Ray, D.; Vorsa, V.; Lineberger, W. C. *J. Phys. Chem.* **1991**, *95*, 8028.
(12) Papanikolas, J. M.; Vorsa, V.; Nadal, M. E.; Campagnola, P. J.; Gord, J. R.; Lineberger, W. C. *J. Chem. Phys.* **1992**, *97*, 7002.
(13) Papanikolas, J. M.; Vorsa, V.; Nadal, M. E.; Campagnola, P. J.; Buchenau, H. K.; Lineberger, W. C. *J. Chem. Phys.* **1993**, *99*, 8733.
(14) Schröder, T.; Schinke, R.; Liu, S.; Bačic, Z.; Moskowitz, J. W. *J. Chem. Phys.* **1995**, *103*, 9228.
(15) Jouvet, C.; Soep, B. *Chem. Phys. Lett.* **1983**, *96*, 426.
(16) Jouvet, C.; Boivineau, M.; Duval, M. C.; Soep, B. *J. Phys. Chem.* **1987**, *91*, 5416.
(17) Wittig, C.; Sharpe, S.; Beaudet, R. A. *Acc. Chem. Res.* **1988**, *21*, 341.
(18) Sivakumar, N.; Hall, G. E.; Houston, P. L.; Hepburn, J. W.; Burak, I. *J. Chem. Phys.* **1988**, *88*, 3692.
(19) Burnett, J. W.; Young, M. A. *Chem. Phys. Lett.* **1994**, *228*, 403.
(20) Young, M. A. *J. Phys. Chem.* **1994**, *98*, 7790.
(21) Young, M. A. *J. Chem. Phys.* **1995**, *102*, 7925.
(22) Zhang, J.; Dulligan, M.; Segall, J.; Wen, Y.; Wittig, C. *J. Phys. Chem.* **1995**, *99*, 13680.
(23) Wang, P. G.; Zhang, Y. P.; Ruggles, C. J.; Ziegler, L. D. *J. Chem. Phys.* **1990**, *92*, 2806.
(24) Fan, Y. B.; Donaldson, D. J. *J. Chem. Phys.* **1992**, *97*, 189.
(25) Fan, Y. B.; Randall, K. L.; Donaldson, D. J. *J. Chem. Phys.* **1993**, *98*, 4700.
(26) Syage, J. A.; Steadman, J. *Chem. Phys. Lett.* **1990**, *166*, 159.
(27) Syage, J. A. *Chem. Phys. Lett.* **1995**, *245*, 605.
(28) Syage, J. A. *J. Chim. Phys.* **1995**, *92*, 248.
(29) Syage, J. A. *Chem. Phys.* **1996**, *207*, 411.
(30) Buntine, M. A.; Baldwin, D. P.; Zare, R. N.; Chandler, D. W. *J. Chem. Phys.* **1991**, *94*, 4672.
(31) Kades, E.; Rösslein, M.; Brühlmann, U.; Huber, J. R. *J. Phys. Chem.* **1993**, *97*, 989.
(32) Kades, E.; Rösslein, M.; Huber, J. R. *J. Phys. Chem.* **1994**, *98*, 13556.
(33) Hagena, O. F. *Z. Phys. D* **1987**, *4*, 291.
(34) Hagena, O. F.; Obert, W. *J. Chem. Phys.* **1972**, *56*, 1793.
(35) Hagena, O. F. Cluster beams from nozzle sources. In *Molecular Beams and Low Density Gas Dynamics*; Wegener, P. P., Ed.; Springer Series in Physical Chemistry: M. Dekker, Inc.: New York, 1974; p 93.
(36) Hagena, O. F. *Surf. Sci.* **1981**, *106*, 101.
(37) Kappes, M.; Schär, M.; Radi, P.; Schumacher, E. *J. Chem. Phys.* **1986**, *84*, 1863.
(38) Kappes, M.; Schär, M.; Schumacher, E.; Vayloyan, P. *Z. Phys. D* **1987**, *5*, 359.
(39) Hagena, O. F. *Rev. Sci. Instrum.* **1992**, *63*, 2374.

(40) Karnbach, R.; Joppien, M.; Stapelfeldt, J.; Wörmer, J.; Möller, T. *Rev. Sci. Instrum.* **1993**, *64*, 2838.
(41) Bucks, U. *J. Phys. Chem.* **1994**, *98*, 5190.
(42) Dubs, M.; Brühlmann, U.; Huber, J. R. *J. Chem. Phys.* **1986**, *84*, 3106.
(43) Dalby, F. W. *Can. J. Phys.* **1958**, *36*, 1336.
(44) Bancroft, J. L.; Hollas, J. M.; Ramsey, D. A. *Can. J. Phys.* **1962**, *40*, 322.
(45) Obi, K.; Matsumi, Y.; Takeda, Y.; Mayama, S.; Watanabe, H.; Tsuchiya, S. *Chem. Phys. Lett.* **1983**, *95*, 520.
(46) Mayama, S.; Egashira, K.; Obi, K. *Res. Chem. Intermed.* **1989**, *12*, 285.
(47) Dixon, R. N.; Noble, M.; Taylor, C. A. *Faraday Discuss. Chem. Soc.* **1981**, *71*, 125.
(48) Dixon, R. N.; Rosser, C. A. *J. Mol. Spectrosc.* **1985**, *110*, 262.
(49) Clouthier, D. J.; Ramsay, D. A. *Annu. Rev. Phys. Chem.* **1983**, *34*, 31.
(50) Job, V. A.; Sethuraman, V.; Innes, K. K. *J. Mol. Spectrosc.* **1969**, *30*, 365.
(51) Moule, D. C.; Walsh, A. D. *Chem. Rev.* **1975**, *75*, 67.
(52) Moore, C. B.; Weisshaar, J. C. *Annu. Rev. Phys. Chem.* **1983**, *34*, 525.
(53) Henke, W. E.; Selzle, H. L.; Hays, T. R.; Schlag, E. W. *J. Chem. Phys.* **1982**, *76*, 1327.
(54) Blatt, A. H. *Organic synthesis, collection*; Wiley: New York, 1969; Vol. 2, p 363.
(55) Andresen, P.; Rothe, E. W. *J. Chem. Phys.* **1985**, *82*, 3634.
(56) Andresen, P. *Ber. Bunsen-Ges. Phys. Chem.* **1985**, *89*, 245.
(57) Brühlmann, U.; Dubs, M.; Huber, J. R. *J. Chem. Phys.* **1987**, *86*, 1249.
(58) Brühlmann, U.; Huber, J. R. *Z. Phys. D* **1987**, *7*, 1.
(59) Keller, B. A.; Felder, P.; Huber, J. R. *J. Phys. Chem.* **1987**, *91*, 1114.
(60) Brühlmann, U.; Huber, J. R. *Chem. Phys. Lett.* **1988**, *143*, 199.
(61) Huber, J. R. *Pure Appl. Chem.* **1988**, *60*, 947.
(62) Docker, M. P.; Ticktin, A.; Brühlmann, U.; Huber, J. R. *J. Chem. Soc., Faraday Trans. 2* **1989**, *85*, 1169.
(63) Greene, C. H.; Zare, R. N. *J. Chem. Phys.* **1983**, *78*, 6741.
(64) Tarte, P. *J. Chem. Phys.* **1952**, *20*, 1570.
(65) Huber, K. P.; Herzberg, G. *Molecular Spectra and Molecular Structure, Constants of Diatomic Molecules*; Van Nostrand: New York, 1979; Vol. IV.
(66) Callear, A. B.; Wood, P. M. *Trans. Faraday Soc.* **1971**, *67*, 3399.
(67) Saito, S.; Takagi, K. *J. Mol. Spectrosc.* **1973**, *47*, 49.
(68) Petersen, J. C.; Vervloet, M. *Chem. Phys. Lett.* **1987**, *141*, 499.
(69) Bodenbinder, M.; Ulic, S. E.; Willner, H. *J. Phys. Chem.* **1994**, *98*, 6441.
(70) Felder, P.; Günthard, Hs. H. *Chem. Phys.* **1982**, *71*, 9.
(71) Kades, E.; Rösslein, M.; Huber, J. R. *Chem. Phys. Lett.* **1993**, *209*, 275.
(72) Veenstra, B. R.; Jonkman, H. T.; Kommandeur, J. *J. Phys. Chem.* **1994**, *98*, 3538.
(73) Barker, J. *Rare Gas Solids*; Academic Press: London, 1976.
(74) Pack, R. T.; Valentini, J. J.; Cross, J. B. *J. Chem. Phys.* **1982**, *77*, 5486.
(75) Chartrand, D. J.; Shelley, J. C.; Le Roy, R. J. *J. Phys. Chem.* **1991**, *95*, 8310.
(76) Bartell, L. S.; Harsanyi, L.; Valente, E. J. *J. Phys. Chem.* **1989**, *93*, 6201.
(77) Bartell, L. S. *J. Phys. Chem.* **1992**, *96*, 108.
(78) Berry, R. S. *J. Chem. Soc., Faraday Trans.* **1990**, *86*, 2343.
(79) Berry, R. S. *J. Phys. Chem.* **1994**, *98*, 6910.
(80) Anderson, J. B. Molecular beams from nozzle sources. In *Molecular Beams and Low Density Gas Dynamics*; Wegener, P. P., Ed.; Marcel Dekker INC.: New York, 1974; p 1.
(81) Farges, J.; Feraudy, M. F.; Raoult, B.; Torchet, G. Argon clusters in a supersonic beam: Size temperature and mass fraction on condensate, in the range 40 to 1000 atoms per cluster. In *Proceedings of the Tenth International Symposium on Rarefied Gas Dynamics*; DFVLR-Press: Porz-Wahn, Germany, 1976.
(82) Grover, J. R.; Walters, E. A. *J. Phys. Chem.* **1986**, *90*, 6201.
(83) Valente, E. J.; Bartell, L. S. *J. Chem. Phys.* **1984**, *80*, 1451.
(84) Emilsson, T.; Germann, T. C.; Gutowsky, H. S. *J. Chem. Phys.* **1992**, *96*, 8830.
(85) Torchet, G.; Feraudy, M.-F.; Raoult, B. *J. Chem. Phys.* **1995**, *103*, 3074.
(86) Simpson, C. J. S. M.; Griffiths, P. T.; Wallaart, H.; Towrie, M. The dynamics of the photolysis of and product ejection from adsorbates on a transparent dielectric surface. In *Proceedings of the 10th International Symposium on Atomic, Molecular, Cluster, Ion and Surface Physics*; Maier, J. P., Quack, M., Eds.; Engelberg/Obwalden: Switzerland, 1996; p 301.
(87) Stephen, K.; Lukas, K. *Viscosity of Dense Fluids*; Plenum Press: New York, 1979.
(88) Buck, U.; Krohne, R. *Phys. Rev. Lett.* **1994**, *73*, 947.
(89) Jortner, J. *Z. Phys. D* **1992**, *24*, 247.
(90) Turner, P. H.; Corkill, M. J.; Cox, A. P. *J. Phys. Chem.* **1979**, *83*, 1473.
(91) Chauvel, J. P.; Friedman, B. Ri.; True, N. S.; Winegar, E. D. *Chem. Phys. Lett.* **1985**, *122*, 175.
(92) Keller, B. A.; Felder, P.; Huber, J. R. *Chem. Phys. Lett.* **1986**, *124*, 135.
(93) Mestdagh, J. M.; Berdah, M.; Dimicoli, I.; Mons, M.; Meynadier, P.; d'Oliveira, P.; Piuzzi, F.; Visticot, J. P.; Jouvet, C.; Lardeux-Dedonder, C.; Martrenchard-Barra, S.; Soep, B.; Solgadi, D. *J. Chem. Phys.* **1995**, *103*, 1013.
(94) Lahmani, F.; Lardeux, C.; Solgadi, D. *Chem. Phys. Lett.* **1986**, *129*, 24.
(95) Brown, H. W.; Pimentel, G. C. *J. Chem. Phys.* **1958**, *29*, 883.
(96) Müller, R. P.; Russegger, P.; Huber, J. R. *Chem. Phys.* **1982**, *70*, 281.
(97) Müller, R. P.; Huber, J. R. *J. Phys. Chem.* **1983**, *87*, 2460.
(98) Müller, R. P.; Huber, J. R. *Rev. Chem. Intermed.* **1984**, *5*, 423.
(99) Müller, R. P.; Murata, S.; Nonella, M.; Huber, J. R. *Helv. Chim. Acta* **1984**, *67*, 953.
(100) Jacox, M. E.; Rook, F. L. *J. Phys. Chem.* **1982**, *86*, 2899.
(101) Napier, I. M.; Norrish, R. G. W. *Proc. R. Soc. London Ser. A* **1967**, *299*, 317.
(102) McGraw, G. E.; Johnston, H. S. *Int. J. Chem. Kinet.* **1969**, *1*, 89.
(103) Wiebe, H. A.; Heicklen, J. *J. Am. Chem. Soc.* **1973**, *95*, 1.
(104) Wiebe, H. A.; Villa, A.; Hellman, T. M.; Heicklen, J. *J. Am. Chem. Soc.* **1973**, *95*, 7.
(105) Sanders, N.; Butler, J. E.; Pasternack, L. R.; McDonald, J. R. *Chem. Phys.* **1980**, *48*, 203.
(106) Zellner, R. *J. Chim. Phys.* **1987**, *84*, 403.
(107) Jenkin, M. E.; Hayman, G. D.; Cox, R. A. *J. Photochem. Photobiol., A: Chem.* **1988**, *42*, 187.
(108) McCaulley, J. A.; Moyle, A. M.; Golde, M. F.; Anderson, S. M.; Kaufman, F. *J. Chem. Soc., Faraday Trans.* **1990**, *86*, 4001.
(109) Frost, M. J.; Smith, I. W. M. *J. Chem. Soc., Faraday Trans.* **1990**, *86*, 1757.
(110) Ohmori, K.; Yamasaki, K.; Matsui, H. *Bull. Chem. Soc. Jpn.* **1993**, *66*, 51.
(111) Dóbé, S.; Lendvay, G.; Szilágyi, I.; Bérces, T. *Int. J. Chem. Kinet.* **1994**, *26*, 887.
(112) Dewar, M. J. S.; Ritchie, J. P.; Alster, J. *J. Org. Chem.* **1985**, *50*, 1031.
(113) McKee, M. L. *J. Am. Chem. Soc.* **1986**, *108*, 5784.
(114) Batt, L.; Milne, R. T.; McCulloch, R. D. *Int. J. Chem. Kinet.* **1977**, *9*, 567.
(115) Engel, V.; Schinke, R.; Hennig, S.; Metiu, H. *J. Chem. Phys.* **1990**, *92*, 1.
(116) Schinke, R.; Hennig, S.; Untch, A.; Nonella, M.; Huber, J. R. *J. Chem. Phys.* **1989**, *91*, 2016.
(117) Nonella, M.; Huber, J. R.; Untch, A.; Schinke, R. *J. Chem. Phys.* **1989**, *91*, 194.
(118) Untch, A.; Weide, K.; Schinke, R. *Chem. Phys. Lett.* **1991**, *180*, 265.
(119) Untch, A.; Schinke, R.; Cotting, R.; Huber, J. R. *J. Chem. Phys.* **1993**, *99*, 9553.
(120) Cox, R. A.; Derwent, R. G.; Kearsey, S. V.; Batt, L.; Patrick, K. G. *J. Photochem.* **1980**, *13*, 149.
(121) JANAF Thermochemical Tables. *J. Phys. Chem. Ref. Data* **1985**, *14*, Supplement 1.
(122) DeMore, W. B.; Sander, S. P.; Golden, D. M.; Molina, M. J.; Hampson, R. F.; Kurylo, M. J.; Howard, C. J.; Ravishankara, A. R. *Chemical Kinetics and Photochemical Data for Use in Stratospheric Modeling*; JPL Publication 90-11990: Jet Propulsion Laboratory: Pasadena, CA, 1990.
(123) Lee, T. J.; Dateo, C. E. *J. Chem. Phys.* **1995**, *103*, 9110.
(124) Dixon, R. N. *J. Chem. Phys.* **1996**, *104*, 6905.
(125) Davidson, J. A.; Thrush, B. A. *J. Chem. Soc., Faraday Trans.* **1975**, *71*, 2413.
(126) Moortgat, G. K.; Šlemr, F.; Warneck, P. *Int. J. Chem. Kinet.* **1977**, *9*, 249.
(127) Jacox, M. E. *J. Phys. Chem.* **1983**, *87*, 4940.
(128) Nielsen, O. J.; Sidebottom, H. W.; Donlon, M.; Treacy, J. *Int. J. Chem. Kinet.* **1991**, *23*, 1095.
(129) Phillips, L. *J. Chem. Soc.* **1961**, 3082.
(130) Levy, J. B. *J. Am. Chem. Soc.* **1953**, *75*, 1801.
(131) Ravishankara, A. R. *Annu. Rev. Phys. Chem.* **1988**, *39*, 367.
(132) Arden, E. A.; Phillips, L.; Shaw, R. *J. Chem. Soc.* **1964**, 5126.
(133) Baker, G.; Shaw, R. *J. Chem. Soc.* **1965**, 6965.
(134) Batt, L.; Milne, R. T. *Int. J. Chem. Kinet.* **1977**, *9*, 549.
(135) Daële, V.; Ray, A.; Vassalli, I.; Poulet, G.; Le Bras, G. *Int. J. Chem. Kinet.* **1995**, *27*, 1121.
(136) Batt, L.; Milne, R. T. *Int. J. Chem. Kinet.* **1977**, *9*, 141.
(137) Balla, R. J.; Nelson, H. H.; McDonald, J. R. *Chem. Phys.* **1985**, *99*, 323.
(138) Ludwig, B. E.; McMillan, G. R. *J. Am. Chem. Soc.* **1969**, *91*, 1085.